PAPER

Status and improvement of CLAM for nuclear application

To cite this article: Qunying Huang 2017 *Nucl. Fusion* **57** 086042

IOP Publishing | International Atomic Energy Agency Nuclear Fusion

Nucl. Fusion **57** (2017) 086042 (9pp) https://doi.org/10.1088/1741-4326/aa763f

Status and improvement of CLAM for nuclear application

Qunying Huang

Key Laboratory of Neutronics and Radiation Safety, Institute of Nuclear Energy Safety Technology, Chinese Academy of Sciences, Hefei, Anhui 230031, People's Republic of China

E-mail: qunying.huang@fds.org.cn

Received 15 December 2016, revised 3 May 2017
Accepted for publication 1 June 2017
Published 14 July 2017

Abstract

A program for China low activation martensitic steel (CLAM) development has been underway since 2001 to satisfy the material requirements of the test blanket module (TBM) for ITER, China fusion engineering test reactor and China fusion demonstration reactor. It has been undertaken by the Institute of Nuclear Energy Safety Technology, Chinese Academy of Sciences under wide domestic and international collaborations. Extensive work and efforts are being devoted to the R&D of CLAM, such as mechanical property evaluation before and after neutron irradiation, fabrication of scaled TBM by welding and additive manufacturing, improvement of its irradiation resistance as well as high temperature properties by precipitate strengthening to achieve its final successful application in fusion systems. The status and improvement of CLAM are introduced in this paper.

Keywords: CLAM, test blanket module, fusion, ITER

(Some figures may appear in colour only in the online journal)

1. A brief introduction on CLAM

Reduced activation ferritic/martensitic (RAFM) steel is considered as one of the most promising candidate structural materials for fusion reactors due to its high strength, high heat conductivity, high resistance to irradiation and low activation features [1–4]. Furthermore, it is selected as the structural material for all six International Thermonuclear Experimental Reactor (ITER) test blanket modules (TBMs). The China low activation martensitic steel (CLAM) development is led by the Institute of Nuclear Energy Safety Technology (INEST), Chinese Academy of Sciences (CAS) with the participation of more than thirty domestic and oversea research units. It has been chosen as the structural material in the design of FDS series PbLi blankets for fusion reactors and China fusion engineering test reactor (CFETR) blanket [5–7]. In particular, it has been chosen as the primary candidate structural material for Chinese helium cooled ceramic breeder (HCCB) TBM for ITER.

Since the TBMs will be tested in ITER, the properties of CLAM have to be evaluated and assessed based on the French regulations on pressure vessel equipment, probably in its nuclear extension, as well as high standards of quality assurance required for reliable and safe operation of ITER [8]. A lot of efforts are being devoted regarding the development of CLAM steel in material fabrication processes, material property evaluations (including mechanical properties, corrosion, irradiation and joining) and the establishment of a material database for its successful application in ITER CN TBM. All of the properties of CLAM are tested in accordance with the RCC-MRx code with the guidance of agreed notified body (ANB). The status of these activities and the improvement of CLAM, such as secondary phase strengthening on CLAM and additive manufacturing, are introduced in this paper.

2. Newly prepared heats of CLAM and properties

2.1. Chemical composition design & fabrication process control

Alloy composition refinement has been an effective method to improve the performance the RAFM steels, such as the evolution of Eurofer 97 [9–13], and F82H [14–18]. More dramatic alloy composition adjustment has also been investigated in CLAM steel. For instance, increasing the percentage of Ta (up to 0.2 wt.%) resulted in the improvements in both

Table 1. Chemical compositions of CLAM (HEAT 1506) (wt.%).

Cr	W	Ta	V	C	Si	Mn	P	S	O	N	Fe
9.11	1.52	0.20	0.19	0.12	0.03	0.41	0.003	0.003	0.001	0.002	Bal.

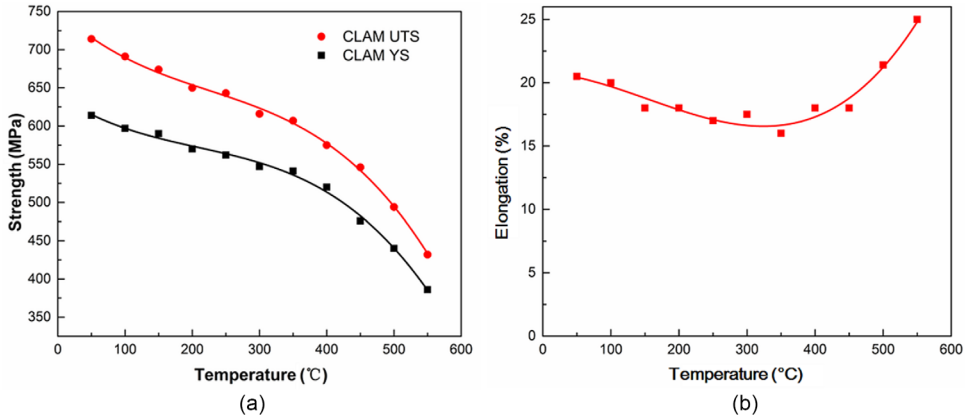

Figure 1. (*a*) Tensile strength and (*b*) total elongation of CLAM (HEAT 1506) under different test temperatures.

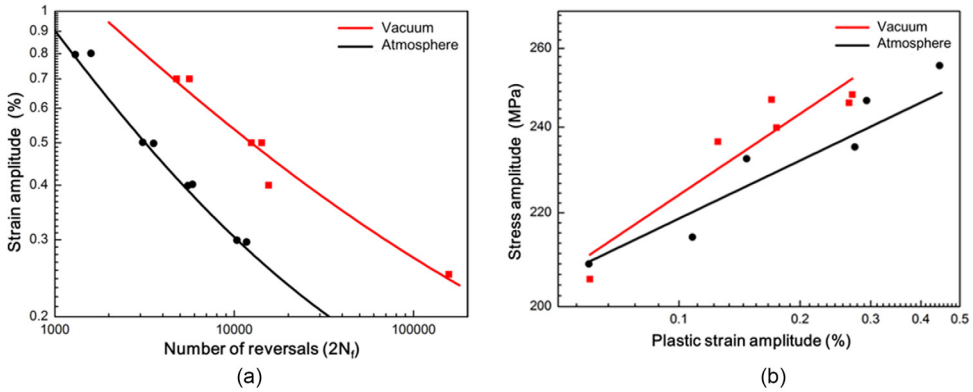

Figure 2. (*a*) Fatigue life and (*b*) cyclic stress–strain curve of CLAM in vacuum and air.

impact properties and creep resistance [19]. Based on this result, an industrial scale ingot of 6.4 tons, nominated as HEAT 1506, was fabricated with vacuum induction melting (VIM) and vacuum arc remelting (VAR). Two types of plates, with the sizes of 7600 mm × 1550 mm × 15 mm and 2100 mm × 1500 mm × 52 mm, were fabricated. The heat treatment is normalizing at 1000 °C for 40 min and then cooling in water, and tempering at 740 °C for 90 min followed by air cooling. Since the HEAT 1506 was prepared and tested for process and property verification of the industrial scale heats for ITER CN TBM qualification, its physical, tensile and fatigue properties have been tested and are presented in this paper, and the other properties (e.g. creep, aging, irradiation and so on) are being tested or scheduled.

The chemical compositions of HEAT 1506 are listed in table 1. Its physical properties, such as elastic and thermal properties, are consistent with the results of previous heats [20] and are not listed here.

2.2. Mechanical properties

2.2.1. Tensile properties. The tensile properties of CLAM (HEAT 1506) were tested at temperatures ranging from 50 °C to 550 °C, as shown in figure 1. Compared with tensile properties of CLAM (HEAT 0408) in [20], the ultimate tensile strength (UTS), 0.2% yield strength (YS) in figure 1(*a*) increased noticeably and the elongation in figure 1(*b*) was similar. These would be caused by the increase in Ta content which enhanced the precipitation of MX phase and refined the grain size [21].

Table 2. Pure fatigue parameters of CLAM in vacuum and air.

Parameter	$\frac{\sigma_f'}{E}$	ε_f'	b	c
Vacuum	0.2954	21.35	−0.069	−0.437
Air	0.2947	63.53	−0.083	−0.645

2.2.2. Fatigue properties. The effect of vacuum environment on the low cycle fatigue (LCF) properties of CLAM (HEAT 1506) was carried out, considering that the blankets are operated in vacuum. Pure fatigue tests were carried out in vacuum ($\leqslant 5 \times 10^{-3}$ Pa) under axial strain at 550 °C. The strain amplitudes ranged from 0.25% to 0.7% with full reversion at 550 °C and all tests were carried out at a strain rate of 2×10^{-3} s^{-1}.

The fatigue properties of CLAM in vacuum and air are shown in figure 2. According to the fatigue life and cyclic

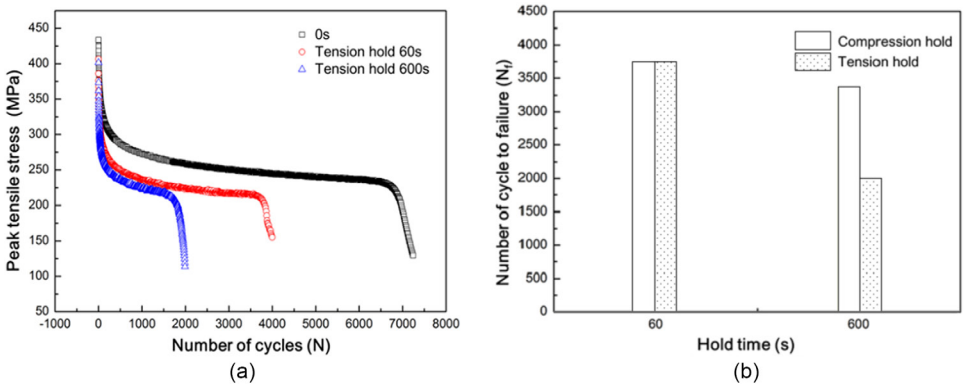

Figure 3. (*a*) Cyclic stress response curves and (*b*) creep-fatigue life of CLAM at different holding times.

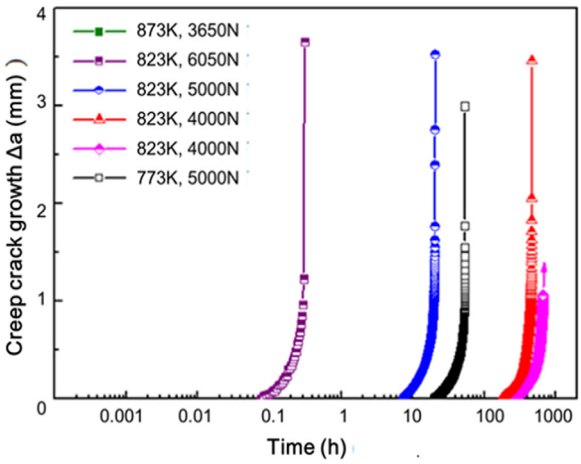

Figure 4. Creep crack growth versus time at different temperatures and loads.

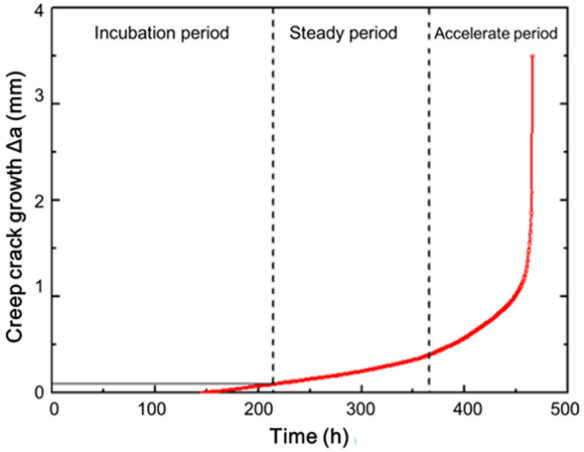

Figure 5. Three stages of creep crack growth curve.

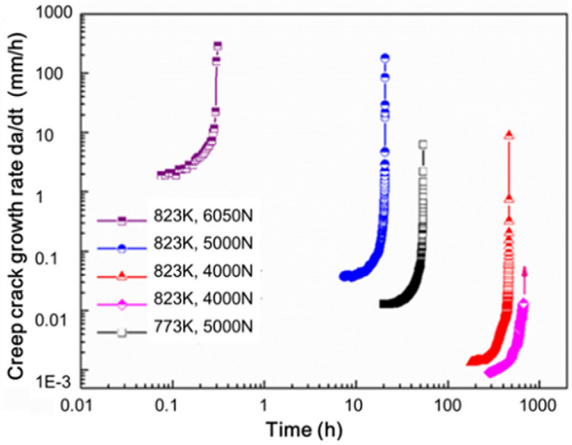

Figure 6. Creep crack growth rate versus time at different temperatures and loads.

stress–strain curve shown in figures 2(*a*) and (*b*), respectively, it is clear that fatigue life increased about one order of magnitude in vacuum than in air at low strain amplitude, and increased by several times at higher strain amplitude. The data satisfied with the Coffin–Manson relation well as the following equation:

$$\frac{\Delta\varepsilon_f}{2} = \frac{\sigma'_f}{E}(2N_f)^b + \varepsilon'_f(2N_f)^c$$

where $\frac{\Delta\varepsilon_f}{2}$ is the total strain amplitude, $2N_f$, $\frac{\sigma'_f}{E}$ and ε'_f are the number of reversals to failure, fatigue strength coefficient and fatigue ductility coefficient, respectively. These parameters are listed in table 2.

During an operation of ITER, the blanket structural material is subjected to pulsed mode plasma loading with peak load holding which will induce creep-fatigue damage. The creep-fatigue behaviour of CLAM in vacuum was thus investigated, as shown in figure 3. Two types of unilateral holding at peak locations of tensile or compressive were conducted with a holding time of 1 min and 10 min, respectively. Cyclic stress response (CSR) curves in figure 3(*a*) showed a gradual softening until complete failure under the creep-fatigue process. Creep-fatigue life in figure 3(*b*) was found to decrease with increasing holding time. In particular, short-time tension and compression holding exhibited no difference on fatigue life in vacuum. Under long-time holding, fatigue life was more sensitive to tension holding, this is opposite to the behaviour in air [22]. In modified 9Cr-1Mo steel, Vani Shankar *et al* [23] also found that the alloy exhibited tensile dwell sensitivity in vacuum and compressive dwell sensitivity in air. It is considered that an oxide coating formed on the surface cracks in air and led to crack tip blunting during the tension holding, but the cracks were shut down during the compression holding and thus they stayed sharp.

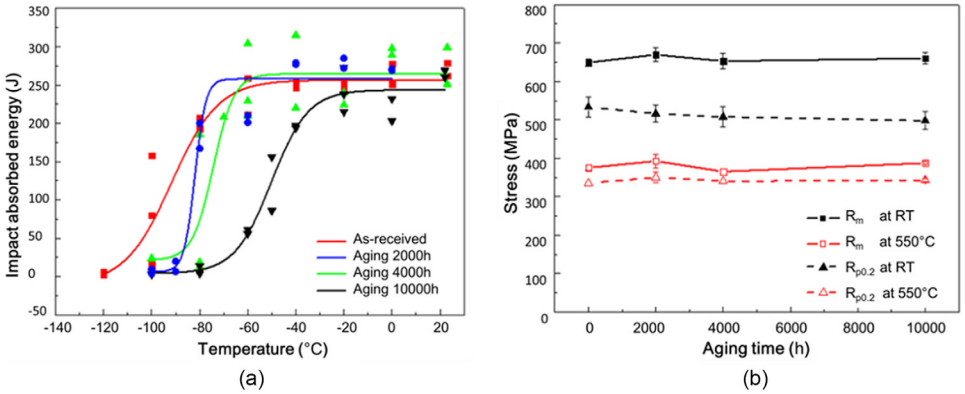

Figure 7. (*a*) Impact and (*b*) tensile properties of CLAM after long-term aging at 550 °C. Reprinted from [25], Copyright 2016, with permission from Elsevier.

Table 3. Chemical compositions of CLAM filler wire (wt.%).

Cr	W	V	Ta	Mn	C	Si	Mo	P	S	Fe
8.15	1.41	0.19	0.13	0.58	0.14	0.06	0.005	0.006	0.003	Bal.

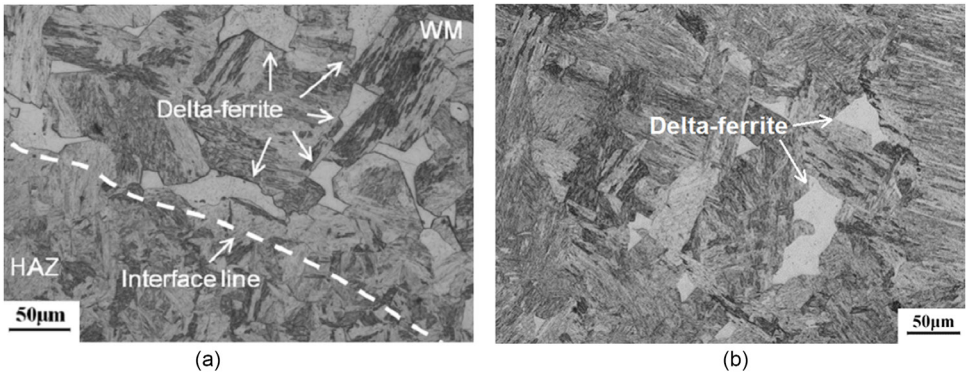

Figure 8. Microstructure in (*a*) the interface of HAZ and WM and (*b*) the centre of WM.

2.2.3. Creep property. The creep crack propagation behaviour of CLAM (HEAT 0912) was studied with the CT specimens at different temperatures. The specimens were 1/4 size compact tension (CT) specimens. A pre-crack of about 2.5 mm long was introduced with a high frequency fatigue testing machine and a side-grooved with 20% of the thickness of the specimen was machined in the sample.

Figure 4 shows the creep crack growth versus time under different testing temperatures and loads. The initial stage of cracking exhibited a transient phenomenon because of the building up of damage at a crack tip prior to the onset of steady state behaviour. The creep crack growth curves showed three stages: incubation period, steady period, and accelerate period (as shown in figure 5). The incubate time significantly increased as the initial load and test temperature decreased. Figure 6 shows the creep crack growth rate of CLAM under different stresses and temperatures. The creep crack growth rate increased with elevating the stress and temperature.

2.2.4. Thermal aging. The aging effect is another key factor related to the design limit of RAFM steel; this is because thermal aging may cause a significant change in the microstructure and degradation of the mechanical properties. Investigation on the microstructure evolution and its impact on mechanical

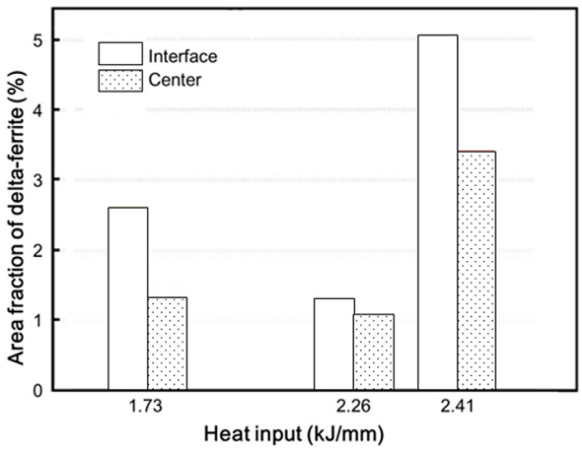

Figure 9. Area fraction of δ-ferrite under different welding conditions.

properties of CLAM (HEAT 0912) were carried out in air at 550 °C for up to 10 000 h, at 600 °C and 650 °C for 5000 h. The DBTT of the thermally-aged CLAM specimens increased to about −46 °C, −10 °C and −20 °C after 10 000 h at 550 °C, 5000 h at 600 °C and 650 °C [24, 25]. The tensile and impact properties of CLAM after aging at 550 °C were given in figure 7, both YS and UTS were not seriously affected by aging,

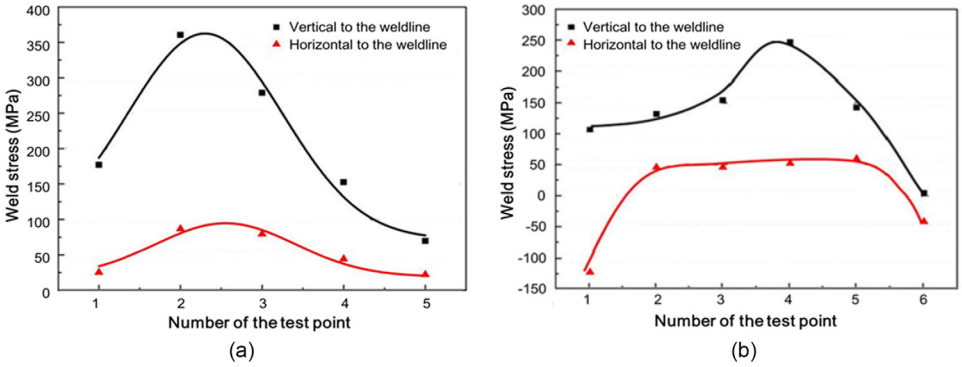

Figure 10. Weld stress distribution along the welding direction with (*a*) constant full constrain by clamps and (*b*) without constrain when the clamps were removed.

and the sizes of $M_{23}C_6$ and the Laves-phase increased during thermal aging [25]. Cavities would nucleate at boundaries next to the large particles and trigger the fracture mode transition from transgranular fracture to intergranular fracture. Moreover, the grain coarsening could cause DBTT to increase [26]. During long-term thermal aging, the $M_{23}C_6$ carbides (60–200 nm) had a strong pinning effect on the migration of the subgrain boundaries. The Laves-phase showed much slower growth kinetics at 650 °C than that at 600 °C. This indicated that the nose temperature of Laves-phase formation in CLAM steel was probably lower than 650 °C. The results showed that the Laves-phase had a small impact on the strength in the early stages of precipitation, but the formation of Laves-phase was detrimental to the impact toughness [4].

2.3. Irradiation tests

To promote the application of CLAM in a high dose neutron irradiation environment, a series of neutron irradiation experiments have been carried out. The fission neutron irradiation experiments on CLAM (HEAT 0912 & HEAT 0603) in the high flux engineering test reactor (HFETR) at Nuclear Power Institute of China (NPIC) reached a dose of 2.98 dpa, which is close to the life-time dose level of RAFM steel in ITER [27]. The spallation neutron irradiation experiments were conducted in the Swiss spallation neutron source (SINQ) in Paul Scherrer Institute (PSI) in Switzerland. Series SINQ target irradiation programs (STIP) in PSI are performed for different materials at different irradiation conditions. The maximum irradiation dose of CLAM (HEAT 0408) in STIP-V was ~21 dpa, which is close to the dose level per year in DEMO [28]. Compared the post neutron irradiation properties of CLAM steel with those of Eurofer 97, F82H and so on in both fission and spallation neutron irradiations [29–33], the results of the two types of irradiation experiments verified that the performance of CLAM after neutron irradiation was similar to those of F82H and Eurofer 97 irradiated under similar irradiation conditions.

Based on these experiences, new projects on neutron irradiation tests of CLAM steel has been made according to the requirements of the fusion reactor engineering application. In the new projects, physical and mechanical properties of CLAM samples irradiated up to ~100 dpa at 300–500 °C in nuclear reactors will be tested following the detailed property requirements of the RCC-MRx code. The neutron irradiation properties of CLAM steel, including specific heat, thermal resistivity, thermal conductivity, Poisson's ratio, creep, fatigue, fracture toughness, tensile, impact, properties of joint and so on, will be obtained with neutron irradiation dose of ~3 dpa and 50–100 dpa gradually to meet the application permission at different steps on the road map of ITER and fusion DEMO reactors in China.

At the same time, several large neutron irradiation facilities have been proposed to evaluate the performance of structural materials for fusion reactors, such as HFETR, HFR, HFIR, SINQ, IFMIF [34] and so on. In addition, the multi-scale modelling for atomic-scale to continuum-scale can be utilized to bridge the phenomena associated with irradiation damage effects of materials in different neutron irradiation facilities.

2.4. Welding

It is a great challenge to fabricate the TBM due to its complex structures. A lot of efforts have been devoted to the weldability of CLAM with different welding technologies such as hot isostatic pressing (HIP) diffusion bonding, tungsten inner gas (TIG) welding, electron beam welding (EBW) and laser beam welding (LBW). According to the Schaeffler constitution diagram, the composition of CLAM shows an obvious tendency to form δ-ferrite in the weld metal (WM), which is detrimental to the impact toughness of the welded joints. Compared to the base metal, the composition of the filler wire was adjusted a little, as listed in table 3, to depress the residual δ-ferrite. CLAM TIG butt welding with modified filler wires of ϕ1.2 mm was conducted to investigate the relationship between the microstructure of the joint and the heat input in the welding. The microstructure at the interface area between the heat affected zone (HAZ) and WM and in the centre of WM are shown in figure 8 and the area fraction of δ-ferrite in the WM with different heat inputs are given in figure 9. The results showed that the δ-ferrite content decreased to ~1% when the heat input was about 2.26 kJ mm^{-1}.

Both of the weld stress distributions along the welding direction with and without the clamps after welding were measured. As shown in figure 10, the weld stress peak value

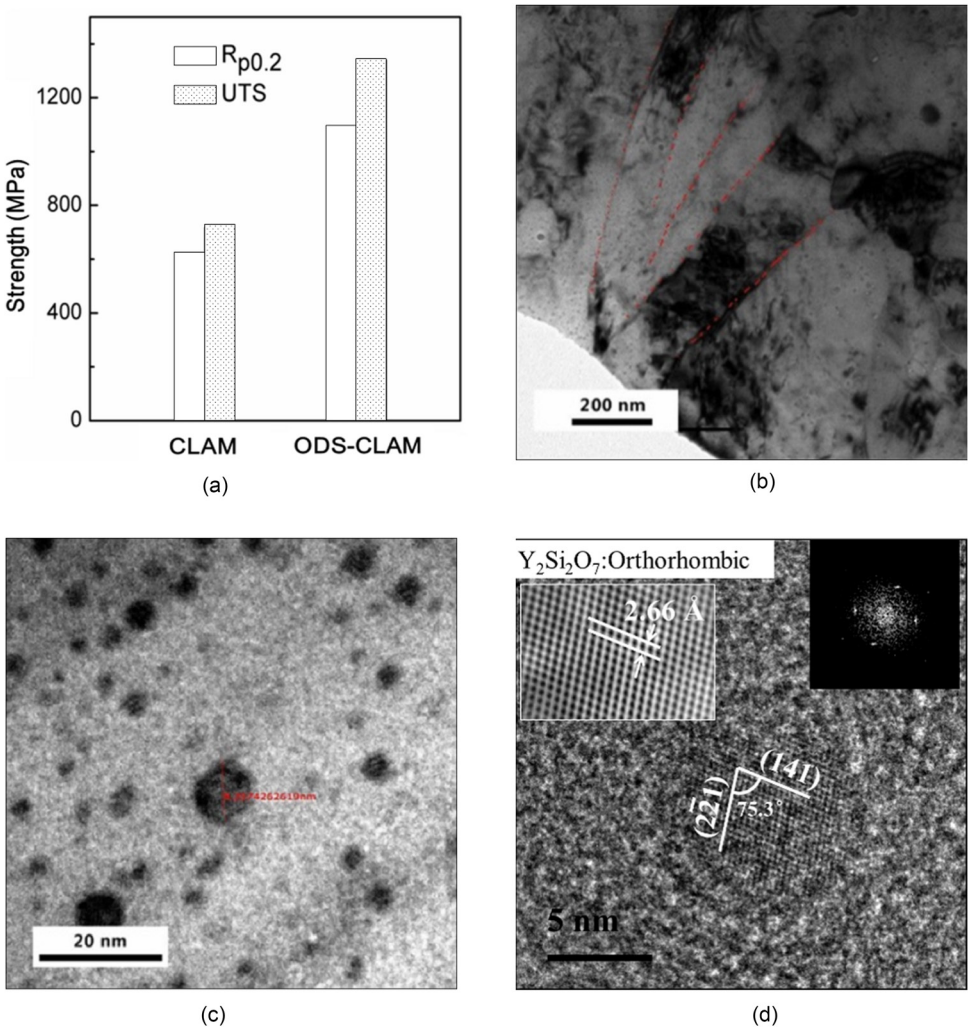

Figure 11. (*a*) Tensile strength of CLAM and ODS-CLAM, and TEM images of ODS-CLAM: (*b*) ultrafine martensitic lath structure, (*c*) the distribution of nano-particles, (*d*) a nano-oxide with a size of ~8 nm.

under constant fully constrained condition was up to 360 MPa, which is nearly 65% of YS of CLAM. After removing the clamps, the weld stress, especially the stress vertical to the weld line reduced noticeably. Even the compression stress horizontal to the weld line was observed at the beginning and end of the weld line. The influence of the weld stress on the microstructure and mechanical properties is being investigated. The systemic research on mechanical properties such as creep and fatigue of the weldments is also planned.

3. Innovative designing theory based on current progress

Current results indicate that RAFM steel roughly fulfils the requirements of ITER based on its strength, creep properties, irradiation resistance and application temperature. However, the operation temperature of structure materials can exceed 600 °C to improve the efficiency of fusion power plants, coupled with the neutron irradiation dose up to 200 dpa. A lot of work is needed to further improve the upper operation temperature and irradiation resistance of CLAM.

3.1. Selective secondary phase strengthening

3.1.1. Thermal stability of precipitates. As it is known, the upper operation temperature of RAFM steel is ~550 °C, and its mechanical strength will decrease rapidly at the elevated temperatures. It is expected that the operation temperature can be improved to over 650 °C or even higher. As the high temperature strength of alloys and steels is highly dependent on the secondary precipitates, thermal stability of precipitates in CLAM is one of the major concerns for improving the properties of CLAM at elevated temperature.

Several types of secondary phases have been identified in CLAM, such as $M_{23}C_6$, MX, Z, Laves phases and so on. The MX phase can stand a much higher temperature, up to over 1000 °C. Strengthening of CLAM by selected precipitates such as TaC is under investigation. There are two methods to improve the phase fraction of TaC in CLAM. The first method is to increase the Ta content. However, too much Ta may lead to the decrease of ductility of CLAM. The effect of Ta content on mechanical properties and ductility is intensively investigated [19, 21], and a Ta content of 0.18 ± 0.02 wt.% was chosen for the production of the 6.4 tons CLAM ingot, which

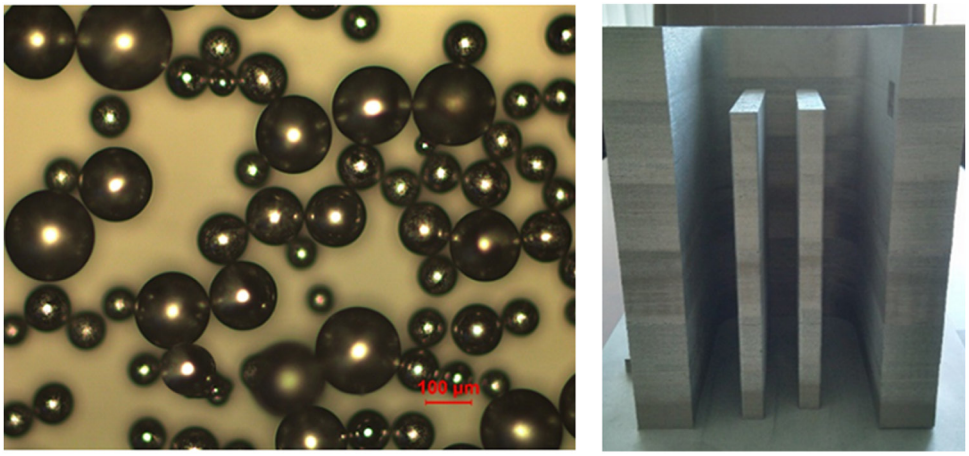

Figure 12. (*a*) CLAM powders and (*b*) scaled first wall of TBM and plates fabricated by SLM.

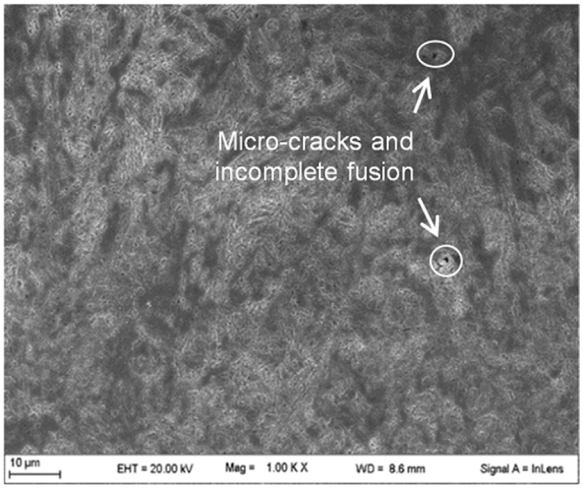

Figure 13. Microstructure of as SLM built CLAM components.

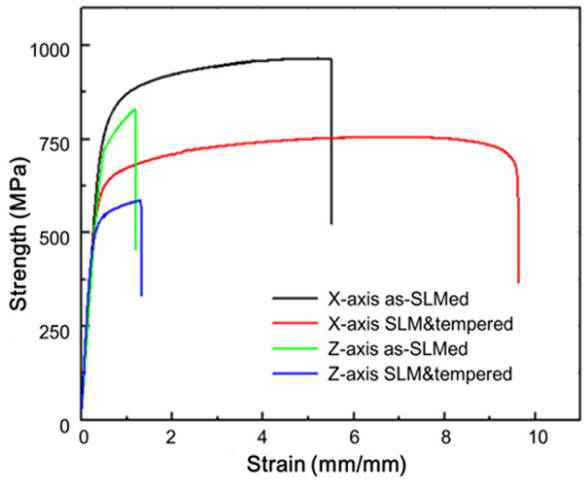

Figure 14. Tensile properties of the SLM built CLAM samples with different heat treatments and directions (*X*-axis: width direction, *Z*-axis: height direction).

demonstrated a higher volume fraction of TaC precipitates and better tensile strength compared with that of a lower Ta content. The other method is to optimize the fabrication process. Thermo-mechanical treatment (TMT) process is being investigated to improve the number density, to reduce the precipitate size and to increase the fraction of MX (i.e. TaC and TaN) precipitates in CLAM.

3.1.2. Irradiation stability. Investigation on the instability of precipitates in F82H steel under ion irradiation showed that the TaC precipitate would dissolve after Fe^{3+} ion irradiation [35]; similar results were observed in other RAFM steels such as the ORNL 9Cr-2WVTa and JLF-1 under neutron irradiation up to 5 dpa at 300 °C [36]. Tan *et al* investigated the stability of MX in ferritic steels under ion irradiation. The results showed that TaC and TaN presented good irradiation stability under a dose of 20 dpa, but the irradiation stability of VN was relatively weaker. The VN nano-precipitates had grown as a rod and presented low number density [37], which was different from TaN and TaC. The N-rich precipitates Ta (C, N) exhibited a noticeably lower stability than TaC during ion irradiation experiments [38].

The stability of precipitates under irradiation is an important factor of high temperature performance for pinning dislocation, martensitic lath boundaries, prior austenitic grain boundaries and so on. However, most ferritic/martensitic steels show obviously weakening at temperatures above 600 °C due to reduced pinning effect of coarsened/dissolved precipitates. Generally, stability of MX-type nano-precipitates, mainly including TaC, TaN and VN, is a key factor to improve strength of RAFM steel at elevated temperatures. Therefore, the amount of TaC should be improved in the next new CLAM while limiting the N-rich precipitates such as VN and Ta (C, N), and the nitrogen content in RAFM steel should be limited for superior performance at high temperature.

3.2. New generation irradiation resistant CLAM steel

To improve the high temperature performance of RAFM steels, the oxide dispersion strengthened (ODS) steels with addition of Y_2O_3 particles based on RAFM steels, such as ODS-Eurofer 97, ODS-F82H, and other 9Cr-ODS steels, have

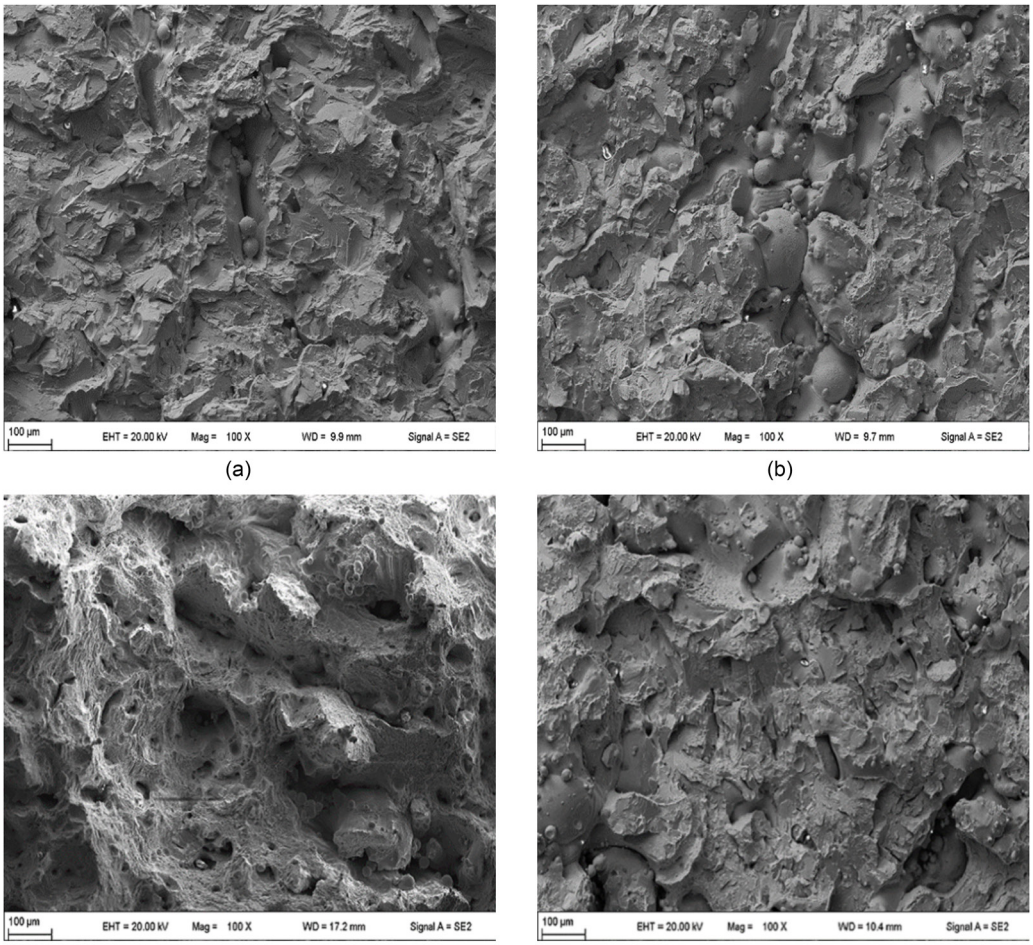

Figure 15. SEM micrographs showing the fracture surfaces of tensile tested samples: as-SLMed in (*a*) length direction and (*b*) height direction; SLMed & tempered in (*c*) length direction and (*d*) height direction.

been developed in Europe, Japan and other countries [39–41]. Nano-oxide particles dispersed inside the matrix act as obstacles to the dislocation motion and significantly improve the creep resistance and neutron irradiation resistance [42, 43]. The ODS steels by addition of thermally stable oxide particles could improve the operating temperature to about 650 °C or even higher temperature [44]. The ODS-CLAM steel was fabricated by mechanical alloying (MA) and HIP with CLAM powder and nano-oxide powders. The microstructural evolutions during the process of ball milling and subsequent consolidating were investigated by SEM, XRD and TEM. The strength of ODS-CLAM was twice as high as CLAM at ambient temperature, mainly due to the ultrafine martensitic-lath structure and the dispersion of nano-sized oxide particles, as shown in figure 11. Further investigation on ODS-CLAM steel is underway, such as optimization of fabrication processes and tests of long-term creep, corrosion, neutron irradiation and so on.

3.3. Microstructure and tensile property of SLMed CLAM

Based on the operation condition of the blanket in the fusion reactor, i.e. high nuclear thermal deposition, the blanket components were usually designed with high density and complex embedded cooling channels to remove the heat. The fabrication of the blanket components by traditional techniques is confronted with great challenges. As the additive manufacturing offers the potential path for fabricating complex and net-shape components, the selective laser melting (SLM) processing, one of the additive manufacturing methods, was employed to investigate the technical feasibility of the manufacturing of ITER CN TBM with CLAM powder, as shown in figure 12. The powder in figure 12(*a*) was produced by the method of atomization comminuting process and its particle size was within 45–105 μm with a mean particle size of 76 μm.

The effect of SLM processing parameters on microstructures and mechanical properties were investigated and the suitable SLM processing window was obtained. As shown in figure 12(*b*), a scaled first wall of TBM with the size of 250 mm (height) × 165 mm (width) × 220 mm (length) and two plates with the size of 100 mm (length) × 12 mm (thickness) × 170 mm (height) for property tests were fabricated. Preliminary measurement indicated that the density of as-built CLAM sample reached 99.7% of the hot-rolled CLAM. The microstructures and mechanical properties were analysed at the conditions of as-SLMed and post-SLM heat treated at 760 °C for 90 min. The results showed that the

microstructures consisted of thin martensitic laths and a small quantity of delta-ferrite, and with the main defects of powders incomplete fusion and micro-cracks, as shown in figure 13.

The results of mechanical properties under various states showed that anisotropic mechanical properties were obvious at as-SLMed and post-SLM heat treated status, as shown in figure 14. The anisotropic properties were mainly demonstrated by a difference in properties between the length direction and height direction, which were only partly reduced by the heat treatment after SLM, and the anisotropic mechanical behaviour was still serious. Additionally, figure 15 shows that fracture failure often occurred at the site of large pores which may have dire effects on the tensile strength.

At present, the most severe problem might be the stress cracking, due to the complex structures of the components and long-term continuous manufacturing. Further work should be focused on the process optimization of SLM and densification in order to reduce the cracking tendency.

4. Summary

Great efforts have been devoted to the research and development of CLAM steel: the mature fabrication process; the material properties, including mechanical properties, corrosion, irradiation, joining and so on, basically met the requirements of TBM.

Newly fabricated 6.4 ton CLAM heat with a slightly higher Ta content and optimized fabrication processes exhibits higher mechanical strength compared with those of the previous CLAM heats. It indicates that the controlled precipitation of secondary phases, such as TaC and TaN, can substantially contribute to the improvement of the properties of CLAM steel. Additional and further testing for the heat is underway based on RCC-MRx for the database of qualification.

A new generation irradiation-resistant CLAM steel is being developed by using TMT processes and nano-oxide dispersion strengthening. It is expected to apply in the environment with higher operation temperature and higher irradiation dose.

Acknowledgments

This work was funded with the National Magnetic Confinement Fusion Science Program of China with Grant Nos. 2013GB108005 and 2015GB109006, and the International Science & Technology Cooperation Program of China with Grant No. 2015DFG62120.

References

[1] Baluc N. *et al* 2007 *Nucl. Fusion* **47** S696–717
[2] Kurtz R.J. *et al* 2009 *J. Nucl. Mater.* **386–8** 411–7
[3] Huang Q.Y. *et al* 2013 *J. Nucl. Mater.* **442** S2–8
[4] Huang Q.Y. and FDS Team 2014 *J. Nucl. Mater.* **455** 649–54
[5] Wu Y.C. and FDS Team 2007 *J. Nucl. Mater.* **367–70** 1410–5
[6] Wu Y.C. and FDS Team 2009 *J. Nucl. Mater.* **386** 122–6
[7] Huang Q.Y. *et al* 2011 *Fusion Eng. Des.* **86** 2611–5
[8] Wu Y.C. *et al* 2016 *Nat. Energy* **1** 16154
[9] Fernández P., Lancha A.M., Lapeña J. and Hernández-Mayoral M. 2001 *Fusion Eng. Des.* **58–9** 787–92
[10] Marmy P. 2007 *J. Nucl. Mater.* **367–70** 86–91
[11] Aktaa J., Weick M. and Petersen C. 2009 *J. Nucl. Mater.* **386–8** 911–4
[12] Giordana M.F., Alvarez-Armas I. and Armas A. 2012 *J. Nucl. Mater.* **424** 247–51
[13] Sandim M.J.R., Farrão F.U., Oliveira V.B., Bredda E.H., Santos A.D., Santos C.A.M. and Sandim H.R.Z. 2015 *J. Nucl. Mater.* **461** 265–70
[14] Sawai T., Shiba K. and Hishinuma A. 2000 *J. Nucl. Mater.* **283–7** 657–61
[15] Sawai T., Wakai E., Tomita T., Naito A. and Jitsukawa S. 2002 *J. Nucl. Mater.* **307–11** 312–6
[16] Schafer L. 2000 *J. Nucl. Mater.* **283–7** 707–10
[17] Maday M.F. 2002 *Fusion Eng. Des.* **61–2** 665–70
[18] Fukumoto K., Sakaguchi T., Inoue K., Itoh T., Sakasegawa H. and Tanigawa H. 2013 *J. Nucl. Mater.* **442** S28–32
[19] Wang K., Liu S.J., Zhai X.W., Zhao Y.Y. and Huang Q.Y. 2016 *J. Fusion Energy* **35** 1–6
[20] Huang Q.Y., Li C.J., Li Y.F., Chen M.L., Zhang M.L., Peng L., Zhu Z.Q., Song Y. and Gao S. 2007 *J. Nucl. Mater.* **367–70** 142–6
[21] Zhai X.W., Liu S.J. and Zhao Y.Y. 2016 *Fusion Eng. Des.* **104** 21–7
[22] Aktaa J. and Petersen C. 2009 *Eng. Fract. Mech.* **76** 1474–84
[23] Shankar V., Bauer V., Sandhya R., Mathew M.D. and Christ H.-J. 2012 *J. Nucl. Mater.* **420** 23–30
[24] Hu X., Huang L.X., Yan W., Wang W., Sha W., Shan Y.Y. and Yang K. 2013 *Mater. Sci. Eng.* A **586** 253–8
[25] Wang W., Liu S.J., Xu G., Zhang B.R. and Huang Q.Y. 2016 *Nucl. Eng. Technol.* **48** 518–24
[26] Zhao M.C., Zeng T.Y., Li J.L., Huang X.F., Zhao Y.C. and Atrens A. 2011 *Mater. Sci. Eng.* A **528** 4217–21
[27] Tavassoli F. 2013 *Proc. Eng.* **55** 300–8
[28] Zinkle S. and Möslang A. 2013 *Fusion Eng. Des.* **88** 472–82
[29] Klueh R.L., Shiba K. and Sokolov M.A. 2009 *J. Nucl. Mater.* **386–8** 191–4
[30] Lucon E., Chaouadi R. and Decréton M. 2004 *J. Nucl. Mater.* **329–33** 1078–82
[31] Rieth M., Dafferner B. and Röhrig H.-D. 1998 *J. Nucl. Mater.* **258–63** 1147–52
[32] Lucon E. and Vandermeulen W. 2009 *J. Nucl. Mater.* **386–8** 254–6
[33] Ge H.E., Peng L., Dai Y., Huang Q.Y. and Ye M.Y. 2016 *J. Nucl. Mater.* **468** 240–5
[34] Knaster J., Moeslang A. and Muroga T. 2016 *Nat. Phys.* **12** 424–34
[35] Tanigawa H., Sakasegawa H., Ogiwara H., Kishimoto H. and Kohyama A. 2007 *J. Nucl. Mater.* **367–70** 132–6
[36] Tanigawa H., Hashimoto N., Sakasegawa H., Klueh R.L., Sokolov M.A., Shiba K., Jitsukawa S. and Kohyama A. 2004 *J. Nucl. Mater.* **329–33** 283–8
[37] Tan L.Z., Katoh Y. and Snead L.L. 2014 *J. Nucl. Mater.* **445** 104–10
[38] Tan L.Z., Byun T.S., Katoh Y. and Snead L.L. 2014 *Acta Mater.* **71** 11–9
[39] Lindau R. *et al* 2005 *Fusion Eng. Des.* **75–9** 989–96
[40] Lindau R., Möslang A., Schirra M., Schlossmacher P. and Klimenkov M. 2002 *J. Nucl. Mater.* **307** 769–72
[41] Wu X.C., Ukai S., Oono N., Hayashi S., Shi S., Chen S.W., Sakasegawa H. and Tanigawa H. 2014 *J. Nucl. Mater.* **452** 212–7
[42] Brocq M., Radiguet B., Poissonnet S., Cuvilly F., Pareige P. and Legendre F. 2011 *J. Nucl. Mater.* **409** 80–5
[43] Lucon E., Leenaers A. and Vandermeulen W. 2007 *Fusion Eng. Des.* **82** 2438–43
[44] Revol S.l, Launois S., Baccino R., Le Marois G. and Rigal B. 2001 *Fusion Eng. Des.* **58–9** 761–5